Extended Frenkel pairs and band alignment at metal-oxide interfaces

O. Sharia,[1] K. Tse,[2] J. Robertson,[2] and Alexander A. Demkov[1,*]
[1]*Department of Physics, The University of Texas at Austin, Austin, Texas 78712, USA*
[2]*Engineering Department, Cambridge University, Cambridge CB2 1PZ, United Kingdom*
(Received 25 September 2008; revised manuscript received 1 February 2009; published 9 March 2009)

We show how oxygen vacancies in metal oxides next to high-work-function metals are stabilized by an oxygen exchange reaction with the metal, and by a charge transfer from the vacancy energy level to the metal Fermi level. The results help explain some of the Fermi-level pinning problems in high-*k* dielectric gate stacks in complimentary metal oxide semiconductor technology and also explain the driving force behind the strong metal-support interaction in oxide-supported catalysts.

DOI: 10.1103/PhysRevB.79.125305 PACS number(s): 73.40.Qv, 71.15.−m, 71.20.−b

I. INTRODUCTION

The adhesion of metal-oxide interfaces is of critical importance for many applications, such as catalysis, oxidation-resistant metals, seals, and thermal barrier coatings.[1–6] It is known that creating interface defects and atomic intermixing will increase the adhesion of such interfaces. In catalysis, a de-activation of certain transition-metal catalysts, known as the strong metal-support interaction,[7,8] has been attributed to the interaction between the metal catalyst and surface defects in the oxide.[9,10] Recently, metal-oxide interfaces have gained a new significance in microelectronics, as the continued scaling of Si field effect transistors (FETs) leads to the use of high dielectric constant (K) oxides such as HfO_2 as a gate dielectric instead of SiO_2, and the use of metals as gate electrodes instead of polycrystalline Si.[11] The gate metals are chosen so that their Fermi levels align to either the conduction-band or valence-band energy of Si, for *n*-FET or *p*-FETs, respectively. However, high-work-function metals such as Pt and Re show an instability in oxygen-deficient conditions, which causes their effective work function (EWF) to shift toward midgap.[12–14] It appears to be related to the presence of oxygen vacancies in the oxide, which modify the interfacial Schottky barrier heights. However, it is unclear why oxygen vacancies are so prevalent, given that their formation energy in HfO_2 is quite large, of order 6.3 eV.[15]

This paper shows that oxygen vacancies are stabilized when created next to a metal by the reaction of the removed oxygen with the metal, and by a charge transfer from the vacancy energy level to the metal. This defect is called an extended Frenkel pair (EFP).[16] The charged vacancy is also attracted by its image charge to the interface. This creates a dipole layer which modifies the Schottky barrier height.

Our previous study of the HfO_2/Mo interface found that the presence of Mo allows the formation of EFPs with the formation energy of only 1.4eV.[16] This leads to a significant density of O vacancies on the HfO_2 side of the interface which modify the effective work function of Mo. This suggests that when searching for a suitable gate metal, the oxidation enthalpy should also be considered in addition to the work-function. In this paper, we report similar studies for two more metals, Rh and Ni. Both of these metals have high work functions, 5.1 eV for Ni and 5.0 eV for Rh. Thus, their work functions are suitable for *p*-type gate electrodes. However, Ni has high oxidation enthalpy like Mo, while Rh has very low value. We find that this difference makes oxygen atoms in HfO_2 more stable if the gate electrode is Rh rather than Ni.

The paper is organized as follows: First we describe theoretical structural models for the HfO_2/Rh and HfO_2/Ni interfaces and discuss their thermodynamic stability and band alignments. Next we consider several EFP defects at these interfaces formed at different distances from the metal. A simple physical model is proposed to explain our results qualitatively.

II. COMPUTATIONAL DETAILS

Theoretical calculations are done within the generalized gradient approximation (GGA) to density-functional theory (DFT). We use the Vanderbilt-type ultrasoft pseudopotentials,[17] supercell geometry and a conventional plane-wave basis set. A $6\times6\times1$ Monkhorst-Pack[18] *k*-point mesh is used for the Brillouin-zone integration. The total energy is converged to 0.005 eV/cell. For larger cells we reduce the number of *k* points proportionately. Atomic positions are relaxed with the conjugate gradient method with force tolerance of 0.05 eV/Å.

For the HfO_2/Rh interface we employ a $5.12\times5.12\times37.39$ Å^3 simulation cell. A kinetic-energy cutoff of 600 eV is found adequate for a well-converged plane-wave basis set [calculations are performed with the Vienna *ab initio* simulation package (VASP) code[19]].The calculations for the HfO_2/Ni interface use a cell of lateral size 7.1×7.1 Å^2, containing seven layers of cubic HfO_2 and five double layers of fcc Ni [calculations are performed with the CASTEP code (Ref. 20)]. A kinetic-energy cutoff of 380 eV is found sufficient.

III. RESULTS

A. Interface geometries

The simplest system is cubic HfO_2/Ni. The Ni and cubic HfO_2 unit cells are lattice matched on their (001) faces, provided that the Ni lattice is rotated by 45 degrees so that [100]HfO_2‖[110]Ni. There are three types of termination of the HfO_2 side; O terminated, stoichiometric, and Hf terminated,[21] as shown in Fig. 1. The stoichiometric interface

 ©2009 The American Physical Society

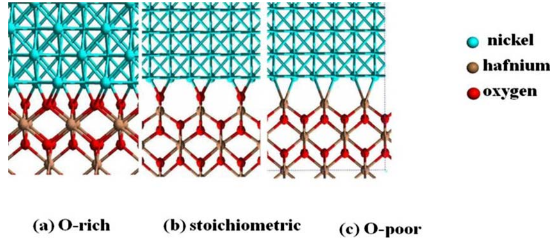

FIG. 1. (Color online) Interface structures for the c-$HfO_2/(100)$Ni interface showing (a) O-rich, (b) stoichiometric, and (c) O-poor (Hf-terminated) interfaces.

is nonpolar. It has 50% of the O atoms of an O-terminated face.

For the HfO_2/Rh interface, we use monoclinic HfO_2. The supercells consist of 15.47 Å of monoclinic hafnia, oxygen-terminated, and (100)-oriented, and 21.89 Å of fcc rhodium as shown in Fig. 2. The lattice constant of Rh(5.34 Å) is about 4% larger than both lateral lattice constants of HfO_2 (a=5.12 Å and b=5.17 Å). We compressively strain Rh laterally to match hafnia. The Rh slab relaxes normally by 3% to accommodate this compressive strain. Note that the $\boldsymbol{a}$ axis of HfO_2 is not perpendicular to [001] plane, the angle β is 99.4°. Therefore, the two HfO_2/Rh interfaces in the supercell are slightly different. Although bond lengths and angles at the two interfaces are very similar, the small difference can result in asymmetric relaxation. However, for most cases there are no problems.

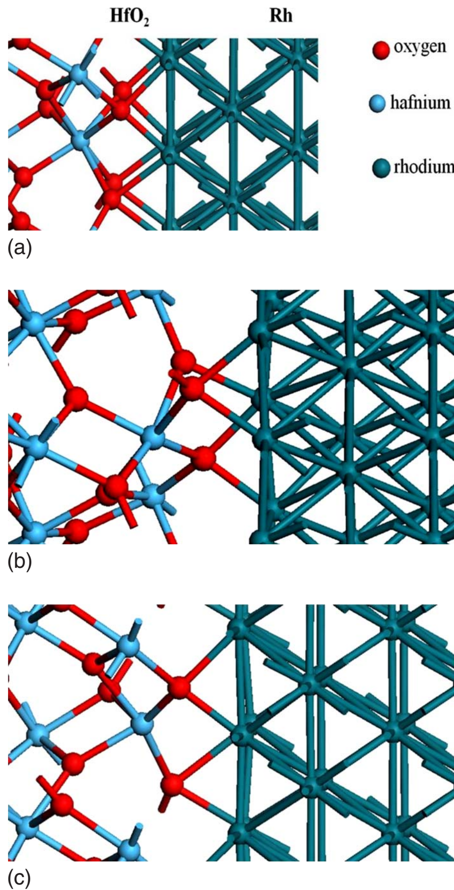

FIG. 2. (Color online) Interface structures of the m-HfO_2/Rh interface. (a) O4, (b) O3, and (c) O2 correspond to four, three, and two oxygen atoms at the interface, respectively. Structure O2 is stoichiometric, both O3 and O4 are oxygen rich.

We consider three different stoichiometries of the HfO_2/Rh interface. The O4 interface has four interface oxygen atoms per surface cell [Fig. 2(a)], structure O3 has three oxygen atoms [Fig. 2(b)], and stoichiometric structure O2 has two [Fig. 2(c)]. After relaxation, the interfacial oxygen atoms in all three structures are fourfold coordinated, making two bonds to Rh and two to Hf. The Rh-O distances range from 1.97 to 2.18 Å, and Rh-O-Rh angles range from 70 to 83°. These bond lengths are similar to those in RhO_2 rutile [2.00 and 2.01 Å (Ref. 22)], while bond angles are significantly smaller (cf. 103° and 128°).

B. Interface energy

The interface energy is estimated using standard thermodynamics.[23,24] The Gibbs free energy at zero temperature is given by

$$\gamma = \frac{1}{2A}[E_{\rm total} - n_{\rm Hf}(E_{\rm Hf} + \mu_{\rm Hf}) - n_{\rm O}(E_{\rm O} + \mu_{\rm O}) - n_{\rm Rh}(E_{\rm Rh} + \mu_{\rm Rh})], \quad (1)$$

where γ is the interface energy, $E_{\rm total}$ is the total energy of the supercell, and A is the interface area. The factor of 2 in equation accounts for two interfaces per supercell. $E_{\rm Hf}$ and $E_{\rm Rh}$ are the total energy per atom of metallic Hf and Rh, respectively. $E_{\rm O}$ is one half of the energy of an oxygen molecule, and $n_{\rm Hf}$, $n_{\rm Rh}$, and $n_{\rm O}$ are the numbers of atoms of each species. $\mu_{\rm Hf}$ and $\mu_{\rm Rh}$ are the chemical potentials with respect to metallic hafnium and say rhodium, respectively. $\mu_{\rm o}$ is the oxygen chemical potential with respect to one half of the oxygen molecule. We impose constraints on the chemical potentials at the interface for equilibrium with the bulk HfO_2 and metallic Rh,

$$2\mu_{\rm O} + \mu_{\rm Hf} = E^f_{\rm HfO2} \quad (2)$$

and

$$m_{\rm Rh} = 0.$$

Here $E^f_{\rm HfO2}$ is the formation enthalpy of hafnia (negative). Using these constraints, we derive the surface energy per unit area as function of the oxygen chemical potential,

$$\gamma = \frac{1}{2A}[E_{\rm total} - n_{\rm Hf}E_{\rm HfO2} - (E_{\rm O} + \mu_{\rm O})(n_{\rm O} - 2n_{\rm Hf}) - E_{\rm Rh}n_{\rm Rh}]. \quad (3)$$

To find the upper and lower limits of $\mu_{\rm O2}$, we use the equilibrium condition at the interface. Oxygen and hafnium atoms prefer forming HfO_2 rather than O_2 molecules and metallic Hf. This means that chemical potentials of oxygen and hafnium are negative. Combining these conditions with Eq. (2) we obtain

$$\frac{1}{2}E^f_{\rm HfO2} < \mu_{\rm O} < 0. \quad (4)$$

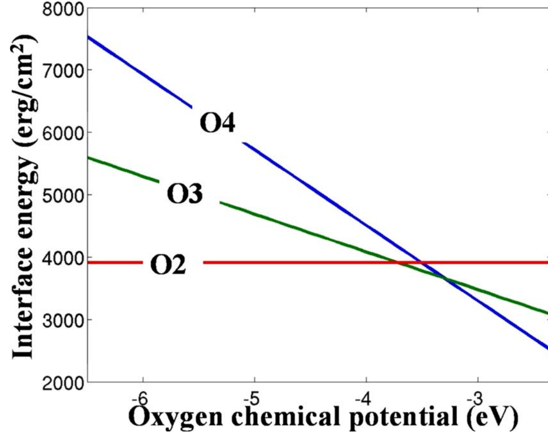

FIG. 3. (Color online) The interface energy as function of the oxygen chemical potential for O4, O3, and O2 structures. The lower limit of the chemical potential is set as a half of the HfO_2 formation energy and the upper limit is a half of the RhO_2 formation energy.

Excluding the possibility of Rh oxidation for now, we can narrow the chemical-potential window even further. Since HfO_2 is in equilibrium with Rh, we can say that oxygen prefers to form HfO_2 rather than RhO_2 (leaving behind residual metallic Hf). Writing this constraint in terms of the chemical potential gives

$$\frac{1}{2}E^f_{\mathrm{HfO2}} < \mu_\mathrm{O} < \frac{1}{2}E^f_{\mathrm{RhO2}}. \quad (5)$$

In Fig. 3 we show the formation energies for three structures. For the oxygen-rich condition O4 is the most stable structure and for the oxygen poor condition O2 is the most stable structure. With two oxygen atoms for every hafnium at the interface O2 is stoichiometric with respect to HfO_2 and its energy is independent of the oxygen chemical potential. There is very a narrow window when O3 structure becomes stable.

C. Band alignment

The band alignment is calculated using the average potential method.[25,26] Figure 4 shows the electrostatic potential for O4 structure averaged in the xy plane. A second macroscopic averaging is used to eliminate the oscillations on the unit-cell scale in the z direction,

$$\bar{V}(z) = \frac{1}{d}\int_{z-d/2}^{z+d/2} V(z')dz'. \quad (6)$$

$V(z)$ is the plane-averaged electrostatic potential and d is the lattice periodicity along z. In Fig. 4, we averaged it separately in the oxide and metal to give a smooth potential across the supercell to use as a reference. In bulk m-HfO_2 (a separate bulk calculation), we find that the valence-band maximum is 2.4 eV above its average electrostatic potential. This places the valence-band maximum of HfO_2 in the supercell. The difference between the Fermi energy and valence-band maximum gives us the valence-band offset (VBO), as indicated in Fig. 4. We find the valence-band offsets are 1.5, 2.0, and 2.5 eV for O4, O3, and O2 interfaces, respectively. The O-rich interfaces have smaller VBOs or larger (n-type) Schottky barriers, or higher EWFs.

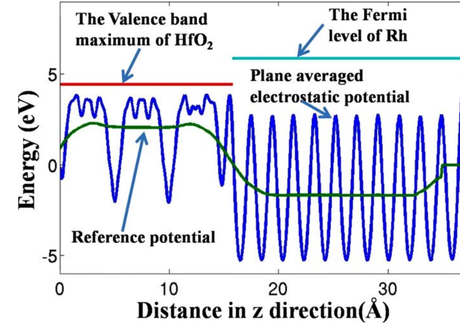

FIG. 4. (Color online) The plane-averaged electrostatic potential for O4 structure in the z direction. From a bulk HfO_2 calculation we determine the valence-band maximum to be 2.4 eV above the average electrostatic potential and use this value to determine the HfO_2 valence-band maximum in the supercell.

The results given in Fig. 4 and Table I are indeed very general,[21] and the effect may be understood as follows. The O2 interface is defined as a nonpolar face of HfO_2 (Ref. 27) so there is no need for a net charge transfer from this face to the metal. Adding extra oxygen to the interface layer, these are not balanced by cations in the oxide so they can only gain electrons from metal atoms in the metal, leaving a O^{2-}-Rh^{+} dipole across the interface. This dipole raises the potential in the oxide, lowers the VBO and increases the EWF.

D. Extended Frenkel pairs

We now consider how the formation of EFPs affects the stability and band offsets at the oxide/metal interface. In other words how the oxygen exchange across the interface modifies the Schottky barrier. To study this problem, we need to consider slightly larger (laterally) cells to eliminate spurious interactions between EFPs. To do so we rotate simulation cells by 45°. The new simulation cell vectors are $\boldsymbol{a}=\boldsymbol{b}$ =7.28 Å, and the angle between them is γ=89.36° (see Fig. 5).

TABLE I. Valence-band offsets and EFP formation energies at the HfO_2/Rh interface (see text).

Structure	$E_{\mathrm{formation}}$ (eV)	VBO (eV)
O4		1.5
O3		2.0
O2		2.5
O4-short	2.77	1.5
O2-short	3.38	2.5
O4-long	3.81	1.8
O3-long	3.87	2.4
O2-long	4.12	2.7
O4-slab	3.60	

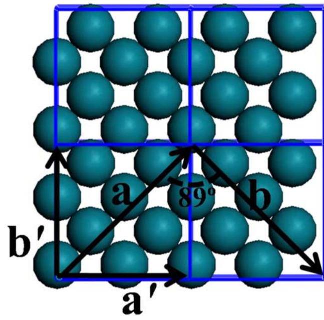

FIG. 5. (Color online) Top view of a simulation cell. Initial cell vectors are $\boldsymbol{a}'$ and $\boldsymbol{b}'$. We choose the new cell vectors $\boldsymbol{a}$ and $\boldsymbol{b}$ along the diagonals of the initial simulation cell.

For each interface structure, there are several options how to create an EFP defect. One can remove oxygen from various places in HfO_2 and can put it in various places in the metal. We first transfer interfacial oxygen into two different places in Rh. First, an oxygen atom is transferred into the Rh layer adjacent to the plane of the interface [referred to as a short EFP, Fig. 6(a)]. Second, the oxygen atom is transferred deeper into the metal [a long EFP, Fig. 6(b)]. Note that there are two interfaces in each simulation cell (due to periodic boundary conditions). Therefore, we must transfer oxygen atoms across both interfaces in a symmetric way. However, after optimization of the atomic positions in the case of the short O3 structure, the atoms did not relax symmetrically but ended up at different depths in Rh, we ignore this case. In all relaxed structures discussed here oxygen atoms in Rh are fourfold coordinated. The average Rh-O distances is 1.85 Å and the Rh-O-Rh angles range from 89° to 119°. The EFP formation energies are summarized in Table I. For O-rich structures the formation energy is smaller than that for stoichiometric interfaces (2.77 eV for short O4 and 3.38 eV for short O2). The formation energy is higher for long EFPs compared to short ones. For a long EFP, the Schottky barrier decreases by $\sim$0.3 eV with respect to the initial interface, while for a short EFP there is almost no effect. This is easily understood in terms of the interface dipole, the long EFP results in a larger charge separation.

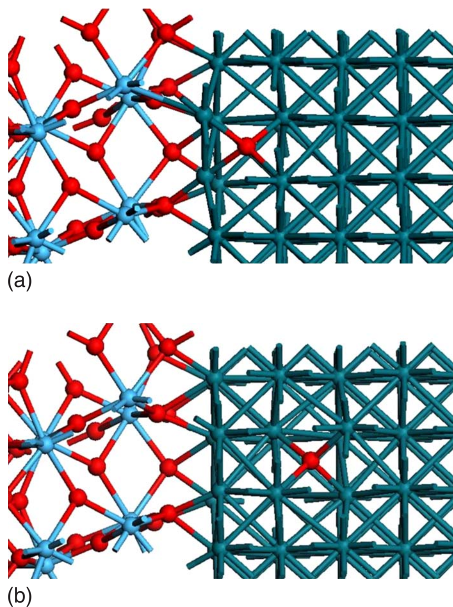

FIG. 6. (Color online) (a) Short and (b) long extended Frenkel pairs for O4 structure of the m-HfO_2/Rh interface. In both cases an interfacial oxygen atom is transferred to Rh. For the short case oxygen is introduced between the first and the second layers of Rh, while for the long case oxygen is transferred to deeper layers.

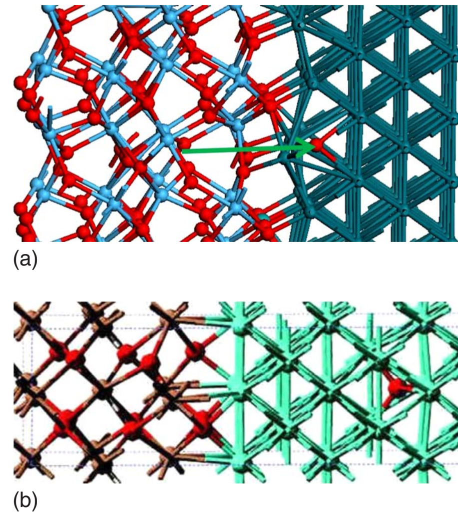

FIG. 7. (Color online) (a) A vacuum slab structure of the O4 m-HfO_2/Rh interface. We transfer one oxygen atom from HfO_2 into Rh. The difference from what is shown in Fig. 6 is that oxygen comes from deeper layers inside HfO_2 not from the interface. (b) Extended Frenkel pair at the c-HfO_2/Ni interface.

The transfer of oxygen from the bulk HfO_2 to Rh in supercell geometry is computationally very demanding. Vacancies in two symmetric positions must be created (to eliminate a spurious electric field), and due to a limited HfO_2 thickness these vacancies will interact with each other. Therefore, we use vacuum slab geometry with 9.7 Å of m-HfO_2, 7.4 Å of Rh, and 17 Å of vacuum. One also worries about the electric field in the oxide created by the charge at the interface. When an oxygen vacancy is created in HfO_2, it leaves behind the +2 charge and causes electron accumulation on the metal side of the interface. For a narrow simulation cell, the field and the interface charge are overestimated. Therefore, we double the width of the initial 5.12×5.12 Å^2 cell to 10.23×10.23 Å^2.

Figure 7(a) shows the transfer of oxygen from HfO_2 to Rh between the first and second metal layers for the O4 interface. The local configuration of oxygen in Rh is slightly different from the previously discussed cases. The Rh-O bond lengths are slightly longer with an average value of 2.0 Å. The formation energy of the EFP is 3.6 eV (O4 slab in Table I), which is almost 1 eV higher than the short EFP. Thus, oxygen atoms in the deeper layers of HfO_2 are more stable with respect to the formation of EFPs than interfacial oxygen atoms. The reason is that oxygen atoms in the interfacial layer do not form proper HfO_2, but rather a mixed oxide HfRhO. Since the enthalpy of oxidation of Rh is lower than that of Hf, interfacial oxygen atoms are easier to remove from such a compound than from stoichiometric HfO_2.

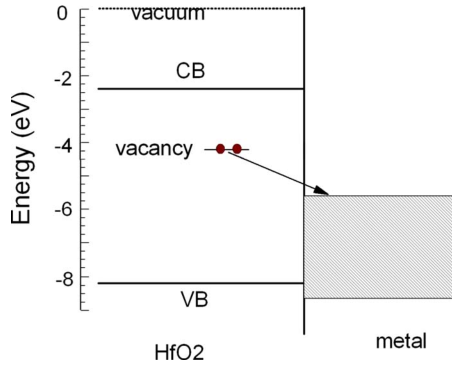

FIG. 8. (Color online) Band model of the extended oxygen Frenkel pair formation, with charge transfer from the vacancy level to the metal.

Overall for the HfO_2/Rh interface we obtain the following results: the stoichiometric interface is most stable with respect to internal oxidation and formation of the EFP defects. The energy required to transfer oxygen atom from the HfO_2 bulk (making this a long EFP) into Rh is 1 eV higher than that required to transfer oxygen from the interfacial layer making O atoms deep in HfO_2 more stable. The formation energy of a short EFP is lower than that of a long EFP. However, the short EFP does not significantly affect the band alignment, while the long EFP increases the VBO by 0.3 eV. Most importantly, owing to the high formation energy of these defects, Rh appears to be a stable *p*-type electrode for HfO_2.

E. HfO_2/Ni interface

Similar results were found for EFPs in the Ni/cubic HfO_2 system [see Fig. 7(b)]. Defects at both O-rich (100) and stoichiometric (100) interfaces (see Fig. 1) were studied. The long EFP with the vacancy well away from a stoichiometric (100) interface costs 3.1 eV. This reduces to 2.7 eV when the vacancy is at the interface. The formation energy for the long EFP at the O-rich (100) interface is more difficult to calculate because of a tendency to be attracted to the interface. It is estimated to be $\sim$1.2 eV. The lower formation energy makes Ni much less attractive gate metal despite its high work function.

The vacancy is attracted to the interface by its image charge when ionized. The VBO for the O-rich interface is less so the energy gain for ionization is larger. This means there is a larger attraction of the O vacancy at the O-rich interface. Also, it seems that the vacancy can diffuse more easily in the calculations in cubic HfO_2 than in *m*-HfO_2 because of the greater order in cubic HfO_2. The difference in formation energies for the O-rich and stoichiometric interface case is consistent with the difference in energy gain from two electrons falling from the vacancy level to the metal Fermi level, as in the simplified model of Sec. III.

IV. DISCUSSION

These results can be understood in terms of a simple model[28] shown in Fig. 8. The oxygen vacancy is created in the HfO_2, and the oxygen is transferred to the metal M to form a unit of that metal oxide denoted MO_n. The overall reaction is

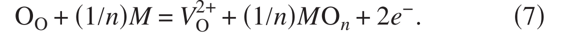

$$O_O + (1/n)M = V_O^{2+} + (1/n)MO_n + 2e^-. \quad (7)$$

The oxygen vacancy in HfO_2 is initially neutral, and it has an energy level in the gap about 3.8 eV above its valence-band edge containing two electrons. These electrons will gain energy by falling to the metal Fermi level. Thus, the formation energy is the sum of four terms,

$$E_{EFP} = E_{form}(V^0) + E_{ox}[(1/n)MO_n] + 2[E(V^0) - E_{F,m}] + V_{es}(d). \quad (8)$$

E_{form} is the formation energy of the neutral vacancy with respect to molecular O_2, the zero chemical potential of oxygen. E_{ox} is the free energy of formation of the oxide MO_n per oxygen atom. The third term is the energy gained by the two electrons falling from the V^0 level to the metal Fermi energy, at infinite separation. V_{es} is the electrostatic contributions to the energy, including the image potential[29,30] between the charged vacancy and its negative image in the metal,

$$V_{image} = \frac{2N^2ed}{\varepsilon_0 \kappa} eV, \quad (9)$$

where N is the areal density of vacancies at distance d from the interface, +2 is their charge, and κ is the dielectric constant of HfO_2 (20–25). This term is of order 0.5 eV. Caution should be used when choosing the dielectric constant of the oxide because screening is enhanced in the close proximity of the metal.[31] The third term will be reduced by the band bending in the oxide due to the other nearby charged defects.

Figure 8 and Eq. (8) explain the much reduced formation energy for O vacancies in HfO_2 when in contact with metals of higher work function. The basic cost of the vacancy 6.3 eV is greatly reduced by the oxide formation and the charge transfer.

Equation (8) explains the difference in EFP formation energies at O-rich and O-poor interfaces. The O-rich interface has a smaller valence-band offset so the energy gain is greater, and the formation energy is smaller. This is seen in Table I.

It is interesting to understand the chemical trends behind Eq. (8) if different metals are used. To do this, we first plot the experimental heats of formation of the metal oxide MO_n per oxygen atom,[32] against the experimental work function of the metal M,[33] as in Fig. 9. There is a clear trend. As expected, less reactive metals have larger work functions and oxides with lower heats of formation. This means that the second and third terms in Eq. (8) oppose each other; the oxide formation energy decreases with increasing WF while the energy gain from electron transfer increases. To zeroth order, the two terms almost balance. Thus Eq. (8), a simplified model and experimental values of oxide free energies and work functions, is found to represent the changes in formation energy between the metals Rh, Ni, and Mo very well.

We can estimate E_{EFP} using Eq. (8), leaving out the image potential term, and the result is plotted in Fig. 10. We see a

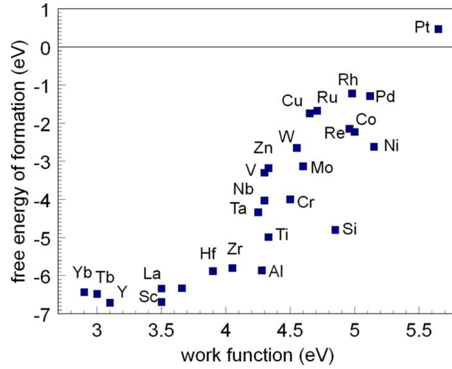

FIG. 9. (Color online) Experimental heat of formation of metal oxides per O atom vs the experimental metal work function.

rather scattered distribution. This arises as follows. Although there is a general trend for larger (negative) oxide formation energies for lower work functions in Fig. 9, the trend is not monotonic. Some elements such as Ni and Si have more stable oxides than expected from their work functions, other such as Rh or Cu have less oxides. Those with less stable oxides have the largest EFP formation energies in Fig. 10.

Detailed calculations show that the EFP formation energy depends on the internal separation of the vacancy and oxygen atom, as in Table I. In addition other groups[34–36] have found that vacancies in Si/HfO_2 supercell structures have a strong tendency to segregate toward the interface (~1.0 eV effect). These effects are a function of both the image charge attraction and chemical bonding. The image charge effect was modeled some time ago by Duffy *et al.*[30] for the metal/TiO_2 system. The energies are smaller in the case of TiO_2 (~0.3 eV) because of its higher dielectric constant (50–60), whereas there is less screening in HfO_2.

In the present study, the formation energy of short EFPs at HfO_2/Rh is less than for those with the vacancy further from the interface ("slab") because the vacancy breaks weak Rh-O bonds as well as strong Hf-O bonds, so it is not to be compared with a bulk vacancy. On the other hand, O vacancies can segregate to the Si/HfO_2 interface because the vacancy can form Hf-Si bonds across the original vacancy for this case. Again, compared to Cho *et al.*,[35] care must be taken in

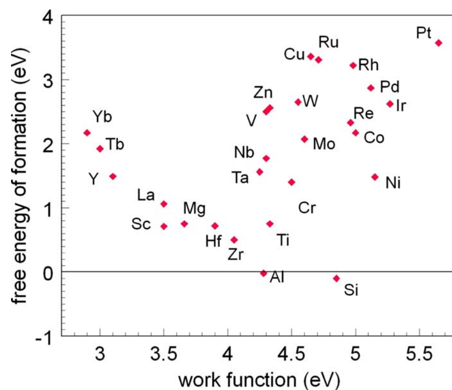

FIG. 10. (Color online) Calculated net formation energy of EFPs from Eq. (8), for various metals on HfO_2 vs the metal work functions.

how energy is assigned, to vacancy formation, relaxation, etc. The V^0 has a small relaxation, but V^{2+} has a large relaxation. Here all our formation energies refer to relaxed vacancies.

A. Application to gate electrodes

In *p*-type FETs in complimentary metal oxide semiconductor (CMOS), we need a gate metal with a high work function of ~5.2 eV. However, according to Eq. (8) this can lead to creation of charged EFPs, which will cause band bending in the oxide and reduce its effective work function. For this application, we need to suppress the vacancy formation. This is best achieved by choosing a metal with the highest EFP formation energy in Fig. 10. Note that the EFP concentration quenched in at some anneal temperature will depend exponentially on this energy so increases of 0.5 eV are useful. We see that the most useful metals are Rh and Ru, those metals with large work functions but whose oxides have a small heat of formation. (Pt and Cu also qualify, but they are undesirable for other reasons.) Mo has often previously been proposed as a *p*-type metal because its (110) face has a large work function of 4.9 eV. However, it has a stable oxide so the EFP formation energy of 1.4 eV is too low.

We see that the net effect of reaction (8) is that even relatively noble metals such as Rh or Ni can reduce stable oxides such as HfO_2. This reaction is more favored for the case when a reaction with Si is allowed, as Si has the most stable oxide for its work function. This was discussed elsewhere.[36–38]

Vacancy formation allows the interfaces to change their stoichiometry. We noted that the O-rich interfaces such as O4 have higher VBOs, and thus smaller EFP formation energies (Fig. 2). This is particularly so for the case of O-rich $HfO_2/Ni(001)$. The resulting O vacancies are attracted toward the interface by their image charge, and there they will start to convert the O-rich interface to a stoichiometric interface. As each vacancy arrives, the stoichiometry falls, the band offset increases, and the formation energy decreases.

B. Application to catalysis

Many metallic catalysts are late transition metals, and the overall catalyst system consists of the metal on an oxide "support."[8] The active sites of a catalyst are the surface sites, as these are higher energy sites of lower coordination. Thus, a more active catalyst is not a continuous thin film on the oxide but well-dispersed nanoparticles. These can be formed by the Volmer-Weber (VW) island growth, rather than Frank van der Merve (FM) layer by layer growth. The observed configuration depends on the surface and interfacial energy of the metal and oxide support via the well-known Young's equation for the metal contact angle.

Metals on the left of the transition-metal series, of low work function, are found to wet the oxide and have FM growth, whereas those to the right, of high work function, are found to de-wet the oxide and have island growth.[9,10] The island growth leads to the more active state. Island growth occurs for Fe, Ni, Ru, Ir, Rh, Pd, and Pt on TiO_2. However, in some circumstances, after heating, an unusual effect oc-

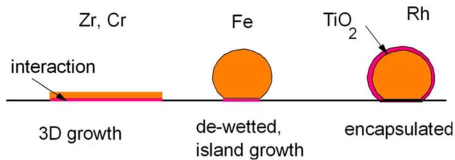

FIG. 11. (Color online) Schematic of metal configurations on TiO_2 supports.

curs. The oxide appears to re-wet the metal and to encapsulate the metal nanoparticles (see Fig. 11). This results in the loss of catalyst activity.[8] The effect is believed to result from an interfacial reduction in the oxide by the metal.[9,10,39]

In normal chemical terms, this reduction is very unusual. The electrochemical series is based on the ordering the elements in terms of more electropositive metals M' being able to displace less electropositive metals from solution or from their oxides MO,

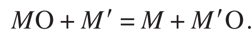

$$MO + M' = M + M'O.$$

Thus, it is not obvious why a noble metal Pt should be able to reduce TiO_2, even at its surface, as Ti is much more electropositive than Pt. The present work shows how this occurs. TiO_2 is the most common support oxide. It is not quite as stable as HfO_2, but the same general principles apply.

Figure 8 shows that an O vacancy can form in the oxide because of the energy gain from the vacancy electrons falling to the metal Fermi level and from the smaller gain in forming the less stable oxide such as RhOx. The point is that the while bulk oxides obey the electrochemical series, an oxide in close contact with a metal can allow some interfacial reduction beyond the electrochemical series, at higher temperatures. The resulting system is a reduced oxide with positively charge vacancies plus a negatively charged metal containing some oxygen. The total system energy has increased. However, the interfacial energy has increased. This now favors a wetting of the metal by the oxide, and metal encapsulation.

In summary, we use density-functional calculations to study the unusual behavior of oxygen vacancies in metal oxides next to high-work-function metals. A simple physical model is proposed explaining the oxygen exchange reaction at the oxide/metal interface, which helps with the gate metal selection for high-k dielectric gate stacks in complimentary metal oxide semiconductor (CMOS) technology and also explains the driving force behind the strong metal-support interaction in oxide-supported catalysts.

ACKNOWLEDGMENTS

This work in part is supported by the National Science Foundation under Grant No. DMR-0548182 and Welch Foundation under Grant No. F-1624. J.R. thanks the J. Tinsley Oden Faculty Foundation for the generous support of his stay in Austin.

*demkov@physics.utexas.edu

[1] M. W. Finnis, J. Phys.: Condens. Matter **8**, 5811 (1996).
[2] U. Schonberger, O. K. Andersen, and M. Methfessel, Acta Metall. Mater. **40**, S1 (1992).
[3] I. G. Batirev, A. Alavi, M. W. Finnis, and T. Deutsch, Phys. Rev. Lett. **82**, 1510 (1999).
[4] A. Bogicevic and D. R. Jennison, Phys. Rev. Lett. **82**, 4050 (1999).
[5] W. Zhang, J. R. Smith, and A. G. Evans, Acta Mater. **50**, 3803 (2002).
[6] X. G. Wang, A. Chaka, and M. Scheffler, Phys. Rev. Lett. **84**, 3650 (2000).
[7] S. J. Tauster, S. C. Fung, and R. L. Garten, J. Am. Chem. Soc. **100**, 170 (1978).
[8] G. L. Haller and D. E. Resasco, Adv. Catal. **36**, 173 (1989).
[9] U. Diebold, J.-M. Pan, and T. E. Madey, Surf. Sci. **331-333**, 845 (1995).
[10] Q. Fu and T. Wanger, Surf. Sci. Rep. **62**, 431 (2007).
[11] J. Robertson, Rep. Prog. Phys. **69**, 327 (2006); J. Vac. Sci. Technol. B **18**, 1785 (2000); E. P. Gusev, V. Narayanan, and M. M. Frank, IBM J. Res. Dev. **50**, 387 (2006).
[12] Y. Liang, J. Curless, C. J. Tracy, D. C. Gilmer, J. J. Schaefer, D. H. Tiyoso, and P. J. Tobin, Appl. Phys. Lett. **88**, 072907 (2006).
[13] J. K. Schaeffer, L. Fonseca, S. Samavedam, D. C. Gilmer, Y. Liang, S. Kalpat, H. H. Tseng, Y. Shiho, A. Demkov, R. Hegde, W. Taylor, D. Triyoso, D. Roan, B. White, and P. Tobin, Tech Dig. – Int. Electron Devices Meet. **2004**, 287.
[14] B. Lee, J. Oh, H. Tseng, R. Jammi, and H. Huff, Mater. Today **9**, 32 (2006); H. C. Wen, P. Majhi, K. Choi, C. S. Park, H. N. Alshareef, H. R. Harris, H. Luan, H. Niimi, H. B. Park, G. Bersuker, P. S. Lysaght, D. L. Kwong, S. C. Song, B. H. Lee, and R. Jammy, Microelectron. Eng. **85**, 2 (2008).
[15] A. S. Foster, F. Lopez Gejo, A. L. Shluger, and R. M. Nieminen, Phys. Rev. B **65**, 174117 (2002).
[16] A. A. Demkov, Phys. Rev. B **74**, 085310 (2006).
[17] D. Vanderbilt, Phys. Rev. B **41**, 7892 (1990).
[18] H. J. Monkhorst and J. D. Pack, Phys. Rev. B **13**, 5188 (1976).
[19] G. Kresse and J. Furthmuller, Phys. Rev. B **54**, 11169 (1996); G. Kresse and J. Futhmuller, Comput. Mater. Sci. **6**, 15 (1996).
[20] M. D. Segall, P. J. D. Lindan, M. J. Probert, C. J. Pickard, P. J. Hasnip, S. J. Clark, and M. C. Payne, J. Phys.: Condens. Matter **14**, 2717 (2002).
[21] K.-Y. Tse and J. Robertson, Phys. Rev. Lett. **99**, 086805 (2007).
[22] M. E. Grillo, Phys. Rev. B **70**, 184115 (2004).
[23] G.-X. Qian, R. M. Martin, and D. J. Chadi, Phys. Rev. B **38**, 7649 (1988).
[24] A. A. Demkov, Phys. Status Solidi B **226**, 57 (2001).
[25] D. M. Bylander and L. Kleinman, Phys. Rev. B **36**, 3229 (1987).
[26] C. G. Van de Walle, Phys. Rev. B **39**, 1871 (1989).
[27] O. Sharia, A. A. Demkov, G. Bersuker, and B. H. Lee, Phys. Rev. B **75**, 035306 (2007).
[28] J. Robertson, O. Sharia, and A. A. Demkov, Appl. Phys. Lett. **91**, 132912 (2007).
[29] A. M. Stoneham and P. W. Tasker, J. Phys. C **18**, L543 (1985).

[30] D. M. Duffy, J. H. Harding, and A. M. Stoneham, J. Appl. Phys. **76**, 2791 (1994).
[31] C. Berthod, N. Binggeli, and A. Baldereschi, Phys. Rev. B **68**, 085323 (2003).
[32] CRC Handbook (2007).
[33] H. B. Michaelson, J. Appl. Phys. **48**, 4729 (1977).
[34] C. Tang and R. Ramprasad, Appl. Phys. Lett. **92**, 182908 (2008).
[35] E. Cho, B. Lee, C. K. Lee, S. Han, S. H. Jeon, B. H. Park, and Y. S. Lin, Appl. Phys. Lett. **92**, 233118 (2008).
[36] P. Broqvist, A. Alkauskas, and A. Pasquarello, Appl. Phys. Lett. **92**, 132911 (2008).
[37] K. Shiraishi, K. Yamada, K. Torii, Y. Akasaka, K. Nakajima, M. Konno, T. Chikyow, H. Kitajima, and T. Arikado, Jpn. J. Appl. Phys., Part 2 **43**, L1413 (2004).
[38] Y. Akasaka, G. Nakamura, K. Shiraishi, N. Umezawa, K. Yamabe, O. Ogawa, M. Lee, T. Amiaka, T. Kasuya, H. Watanabe, T. Chikyow, F. Ootsuka, Y. Nara, and K. Nakamura, Jpn. J. Appl. Phys., Part 2 **45**, L1289 (2006).
[39] Q. Fu, T. Wagner, S. Olliges, and H. D. Carstanjen, J. Phys. Chem. B **109**, 944 (2005).